Synthesis and characterization of novel Ge doped Sr1−yCayFeO3−δ SOFC cathode materials

Porras, Jose; Marco, Jose F.; Berry, Frank J.; Slater, Peter R.

DOI:
10.1016/j.materresbull.2015.02.014

Document Version
Publisher's PDF, also known as Version of record

Citation for published version (Harvard):
Porras, J, Marco, JF, Berry, FJ & Slater, PR 2015, 'Synthesis and characterization of novel Ge doped Sr1−yCayFeO3−δ SOFC cathode materials', *Materials Research Bulletin*, vol. 67, pp. 63-69. https://doi.org/10.1016/j.materresbull.2015.02.014

Materials Research Bulletin 67 (2015) 63–69

Contents lists available at ScienceDirect

Materials Research Bulletin

journal homepage: www.elsevier.com/locate/matresbu

Synthesis and characterization of novel Ge doped $Sr_{1-y}Ca_yFeO_{3-\delta}$ SOFC cathode materials

Jose M. Porras-Vazquez [a,*], Jose F. Marco [b], Frank J. Berry [a], Peter R. Slater [a,*]

[a] School of Chemistry, University of Birmingham, Birmingham B15 2TT, UK
[b] Instituto de Química Física "Rocasolano", CSIC, Serrano 119, Madrid 28006 Spain

ARTICLE INFO

Article history:
Received 16 May 2014
Received in revised form 21 November 2014
Accepted 3 February 2015
Available online 4 February 2015

Keywords:
SOFC
Cathode
Germanium
Ferrite
Perovskite

ABSTRACT

In this paper we report the successful incorporation of germanium into $Sr_{1-y}Ca_yFeO_{3-\delta}$ perovskite materials for potential applications as electrode materials for solid oxide fuel cells. It was observed that Ge doping leads to a change from a tetragonal cell (with partial ordering of oxygen vacancies) to a cubic one (with the oxygen vacancies disordered). Annealing experiments in $5\%H_2/95\%N_2$ (up to 800 °C) also showed the stabilization of the cubic form in reducing conditions for the 15 mol% Ge-doped $SrFeO_{3-\delta}$ sample, in contrast to the undoped systems which showed a transition to an oxygen vacancy ordered brownmillerite-type phase. In order to examine the potential of these systems as SOFC cathodes, composite electrodes comprising 50% $Ce_{0.9}Gd_{0.1}O_{1.95}$ and 50% $Sr_{1-y}Ca_y(Fe/Ge)O_{3-\delta}$ on dense $Ce_{0.9}Gd_{0.1}O_{1.95}$ pellets were examined in air. The results showed an improvement in the area specific resistances (ASR) values for the Ge-doped samples with respect to the undoped ones, with the best performance for the Ge doped $SrFeO_{3-\delta}$ system (0.24 and 0.06 $\Omega\,cm^2$ at 700 and 800 °C, respectively, for $SrFe_{0.85}Ge_{0.15}O_{3-\delta}$). Thus, the results show that germanium can be incorporated into $Sr_{1-y}Ca_yFeO_{3-\delta}$-based materials leading to materials with potential for use as cathode materials in solid oxide fuel cells (SOFC).

1. Introduction

Perovskite transition metal oxides have attracted considerable interest due to potential applications as cathode materials in the field of solid oxide fuel cells (SOFCs) [1–5]. An interesting aspect of the perovskite structure is the ability to accommodate a wide range of dopant sizes, and an unusual consequence of this has been prior observations on the successful incorporation of oxyanions into perovskite-type cuprate superconductors and related phases [6–14]. Such studies demonstrated that the perovskite structure could incorporate significant levels of oxyanions (carbonate, borate, nitrate, sulfate, phosphate), with the C, B, N, P, S of the oxyanion group residing on the perovskite B cation site, while the oxide ions of this group fill 3 (C, B, N) – 4 (P, S) of the available 6 oxide ion positions around this site, albeit displaced so as to achieve the required geometry for the oxyanion. Following on from these earlier observations in the superconductivity field, recently we have illustrated the potential of this oxyanion doping strategy in perovskite-type electrode and electrolyte materials of relevance to applications in solid oxide fuel cells [15–22]. In the electrode area for instance, borate, phosphate and sulphate were successfully incorporated into different cathode materials such as $SrCoO_{3-\delta}$, $La_{1-x}Sr_xCo_{0.8}Fe_{0.2}O_{3-\delta}$, $Ba_{1-x}Sr_xCo_{0.8}Fe_{0.2}O_{3-\delta}$, $CaMnO_3$ and $La_{1-x}Sr_xMnO_3$-type materials, leading to stabilization of high symmetry structures, as well as enhancements of both the electronic conductivity and the electrode performance with respect to the parent compounds. Similarly silicate incorporation has also been demonstrated in $Sr_{1-y}Ca_yMn_{1-x}Si_xO_{3-\delta}$ cathode materials, with direct evidence for the incorporation of Si into the structure provided for the first time by ^{29}Si NMR [23,24]. The successful incorporation of silicate into $SrFeO_{3-\delta}$ has also been recently reported, with improvements in the properties also reported [25,26]. These studies are also of interest to earth science, since Si and Fe containing perovskites, such as $(Mg,Fe)SiO_3$, $(Ca,Fe)SiO_3$, $Ca(Si,Fe)O_{3-\delta}$, have attracted considerable interest due to their accepted presence at the very high pressures in the earth's interior [27–30]. In contrast to these latter studies, the successful incorporation of Si into $Sr_{1-y}Ca_yFeO_{3-\delta}$ at ambient pressure suggests a more widespread ability of the perovskite structure to accommodate Si. Given the interest in Si incorporation in perovskites in earth science, related Ge containing systems have

* Corresponding authors. Tel.: +44 01214148672; fax: +44 01214144403.
E-mail addresses: j.m.porras@bham.ac.uk (J.M. Porras-Vazquez), p.r.slater@bham.ac.uk (P.R. Slater).

http://dx.doi.org/10.1016/j.materresbull.2015.02.014

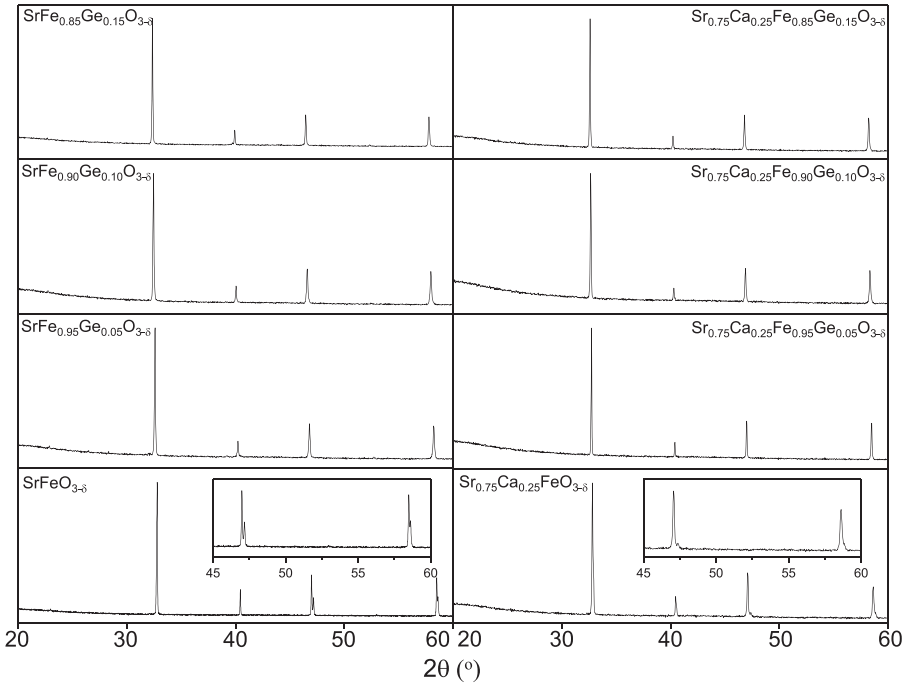

Fig. 1. X-ray diffraction patterns for: (left) $SrFe_{1-x}Ge_xO_{3-\delta}$ and (right) $Sr_{0.75}Ca_{0.25}Fe_{1-x}Ge_xO_{3-\delta}$, showing the stabilization of the cubic form of these series through germanium doping. The insets show the expanded region from 45 to 60° 2θ for $SrFeO_{3-\delta}$ and $Sr_{0.75}Ca_{0.25}FeO_{3-\delta}$ to highlight the lower symmetry of the undoped systems.

also attracted attention, again through high pressure synthesis [31,32]. In terms of ambient pressure synthesis, only two Ge containing perovskite systems have been reported, $LaMg_{0.5}Ge_{0.5}O_3$ and $LaNi_{0.5+x}Ge_{0.5-x}O_3$ [33]. In these systems, structural studies have shown that Ge is accommodated as an octahedral ion. In this work, we investigate whether further Ge containing perovskites can be prepared through an investigation into the possible incorporation of Ge into $Sr_{1-y}Ca_yFeO_{3-\delta}$, a system that has attracted significant interest for use in electrochemical devices such as oxygen permeation membranes, and SOFCs [34–36]. In $Sr_{1-y}Ca_yFeO_{3-\delta}$, iron cations have a mixed valence state with an average oxidation state between +4 and +3, corresponding to a wide range of oxygen nonstoichiometry, and the structure changes from tetragonal to orthorhombic brownmillerite type, as the iron oxidation state reduces to 3+ and hence the composition changes to $(Sr/Ca)FeO_{2.5}$ (with associated long range ordering of oxide ion vacancies) [37–39]. In terms of applications, the formation of ordered oxygen vacancies is not favourable because it drastically reduces oxide ion conduction, while the oxygen deficiency also results in a decrease in both the mobility and concentration of hole carriers [40,41]. In this work, we have therefore investigated whether Ge can be accommodated into these systems, and the consequent effect on the oxygen vacancy ordering and electrode performance.

2. Experimental

$SrCO_3$ (Aldrich, 99.9%), $CaCO_3$ (Aldrich, 99%), Fe_2O_3 (Fluka, 99%) and GeO_2 (Aldrich, 99.999%), were used to prepare $Sr_{1-y}Ca_yFe_{1-x}Ge_xO_{3-\delta}$ ($y = 0$, 0.25 and 0.5; $x \leq 0.15$). The powders were intimately ground and heated initially to 1100 °C for 12 h. They were then ball-milled (350 rpm for 1 h, Fritsch Pulverisette 7 Planetary Mill) and reheated to 1150 °C for a further 12 h. Finally, they were then ball-milled (350 rpm for 1 h) and reheated to 1200 °C for a further 12 h.

Initial phase identification and unit cell parameter determination was carried out by Rietveld profile refinement using powder X-ray diffraction data (XRD) collected on a Bruker D8 diffractometer (Cu Kα_1 radiation).

Analysis of the X-ray diffraction data by the Rietveld method was done using the General Structure Analysis System GSAS [42].

Oxygen contents were estimated from thermogravimetric analysis (Netzsch STA 449 F1 Jupiter Thermal Analyser). Samples were heated at 10 °C/min–1200 °C in N_2 and held for 30 min to reduce the Fe oxidation state to 3+, with the original oxygen content and average Fe oxidation state then being determined from the mass loss observed.

To determine the potential use of these materials as SOFC anodes the samples where annealed for 24 h at 600 or 800 °C in 5% H_2–95%Ar to study the effect of germanium doping on the stability under reducing conditions.

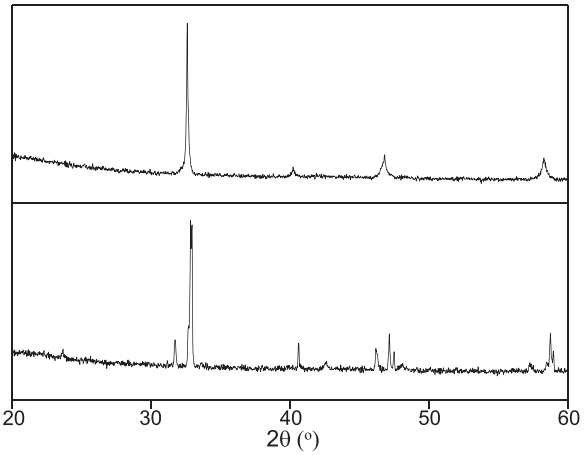

Fig. 2. X-ray diffraction patterns for (a) $Sr_{0.5}Ca_{0.5}FeO_{3-\delta}$ and (b) $Sr_{0.5}Ca_{0.5}Fe_{0.85}Ge_{0.15}O_{3-\delta}$, where it is seen that the cubic form cannot be fully stabilized for high Ge contents for this series: close inspection of the X-ray diffraction patterns showing some evidence for peak broadening/splitting particular for high angles for $Sr_{0.5}Ca_{0.5}Fe_{0.85}Ge_{0.15}O_{3-\delta}$.

Table 1
Unit cell parameters and normalised cell volumes from XRD data for $Sr_{1-y}Ca_yFe_{1-x}Ge_xO_{3-\delta}$. All the doped samples were refined in a cubic cell (P m −3 m) and the undoped samples were refined in a tetragonal cell (I 4/m m m).

Ca (y)	0				0.25			
Ge (x)	0	0.05	0.10	0.15	0	0.05	0.10	0.15
a (Å)	10.9235(1)	3.8738(1)	3.8899	3.9007	10.8895(1)	3.8590(1)	3.8677(1)	3.8749(1)
b (Å)	–	–	–	–	–	–	–	–
c (Å)	7.6965(1)	–	–	–	7.7083(1)	–	–	–
V/Z (Å^3)	57.40(1)	58.13(1)	58.86(1)	59.35(1)	57.12(1)	57.47(1)	57.86(1)	58.18(1)

In order to gather further information on the Fe oxidation state, ^{57}Fe Mössbauer spectra were recorded in constant acceleration mode using a ca. 25mCi ^{57}Co/Rh source and a helium closed-cycle cryo-refrigerator. All the spectra were computer fitted and the chemical isomer shift data are quoted relative to metallic iron at 298 K.

Pellets for conductivity measurements were prepared as follows: the powders were first ball-milled (350 rpm for 1 h), before pressing (200 MPa) as pellets and sintering at 1200 °C for 12 h. Four Pt electrodes were attached with Pt paste, and the sample was fired to 800 °C in air for 1 h to ensure bonding to the sample. The samples were then furnace cooled to 350 °C in air and held at this temperature for 12 h to ensure full oxygenation. Finally, their conductivities were measured using the four probe dc method in air.

To elucidate the potential of these materials for use as SOFC cathodes, symmetrical electrodes were coated on both sides of dense $Ce_{0.9}Gd_{0.1}O_{1.95}$ (CGO10, Aldrich) pellets (sintered at 1500 °C for 12 h) using a suspension prepared with a mixture of electrolyte and electrodes (1:1 wt%) and DecofluxTM (WB41, Zschimmer and Schwarz) as binder material. The symmetrical cells were fired at 900 °C for 1 h in air. Afterwards, a Pt-based ink was applied onto the electrodes to produce a current collector layer and finally the pellets were fired at 800 °C for 1 h. Area-specific resistance (ASR) values were then obtained under symmetrical air atmosphere in a two electrode configuration. AC impedance spectra of the electrochemical cells were collected using a HP4912A frequency analyser, at open circuit voltage (OCV), in the 5 Hz–13 MHz frequency range with ac signal amplitude of 100 mV. The spectra were fitted to equivalent circuits using the ZView software [43] which allows an estimation of the resistance and capacitance associated with the different cell contributions.

3. Results and discussion

3.1. Solid solution range

For the $Sr_{1-y}Ca_yFe_{1-x}Ge_xO_{3-\delta}$ series ($y = 0$, 0.25 and 0.5), single phase samples could be achieved up to 15% germanium substitution, i.e. $x \leq 0.15$ (Figs. 1 and 2). Exceeding this Ge content led to the segregation of secondary phases, such as Sr_2GeO_4 (PDF 47-0113). The undoped samples showed a tetragonal symmetry, indicating some degree of oxygen ordering. Through Ge doping the X-ray diffraction results showed an evolution to a cubic cell, where fully cubic symmetry is obtained at $x = 0.15$ for $y = 0$ and 0.25. The observed change to cubic symmetry from the X-ray diffraction results suggests a decrease in the oxygen vacancy ordering, although further neutron diffraction studies are required to add confirmation to this. For higher Ca contents ($y \geq 0.5$), it does not, however, appear to be possible to fully stabilise the cubic cell symmetry at any germanium content under these ambient pressure synthesis conditions (see Fig. 2). These results agree with previous works where it was demonstrated that oxyanion doping led to a change in the oxygen vacancy ordering, and, thus, in the symmetry [15–18,25]. The addition of higher levels of germanium in this series led to the segregation of secondary phases.

Unit cell parameters for these materials were determined from the X-ray diffraction data using the Rietveld method (see Table 1), and show an increase in the cell volume as the Ge content increases. Similar results were reported in a previous work where

Table 2
Oxygen deficiencies (δ), Fe oxidation states (from TGA), conductivity data and ASR values at 700 °C and 800 °C in air for $Sr_{1-y}Ca_yFe_{1-x}Ge_xO_{3-\delta}$ series. The error estimated for the oxygen deficiencies and iron oxidation states from the noise of the TGA line are ±0.01 and ±0.02, respectively.

	$Sr_{1-y}Ca_yFe_{1-x}Ge_xO_{3-\delta}$			
Ca (y)	0		0.25	
Ge (x)	0	0.15	0	0.15
Oxygen deficiency (δ)	0.10	0.21	0.12	0.18
Oxidation state	3.80	3.53	3.77	3.56
Conductivity at 700 °C (S cm^{-1})	26.3	13.6	8.25	9.63
Conductivity at 800 °C (S cm^{-1})	17.2	9.5	6.69	6.9
ASR at 700 °C (Ω cm^2)	1.65	0.24	0.91	0.62
ASR at 800 °C (Ω cm^2)	0.25	0.06	0.15	0.06

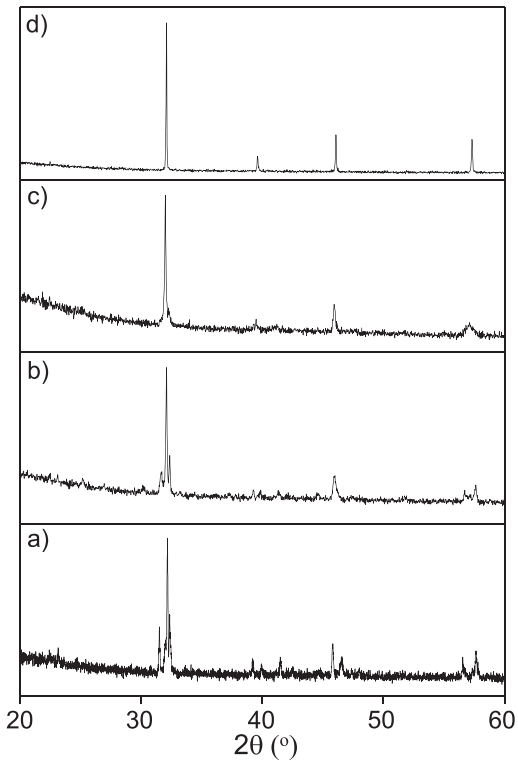

Fig. 3. X-ray diffraction patterns for (a) $SrFeO_{3-\delta}$, (b) $SrFe_{0.95}Ge_{0.05}O_{3-\delta}$, (c) $SrFe_{0.90}Ge_{0.10}O_{3-\delta}$ and (d) $SrFe_{0.85}Ge_{0.15}O_{3-\delta}$, annealed at 800 °C for 24 h in 5%H_2–95%N_2, showing a stabilisation of the cubic phase under these conditions on increasing the Ge content.

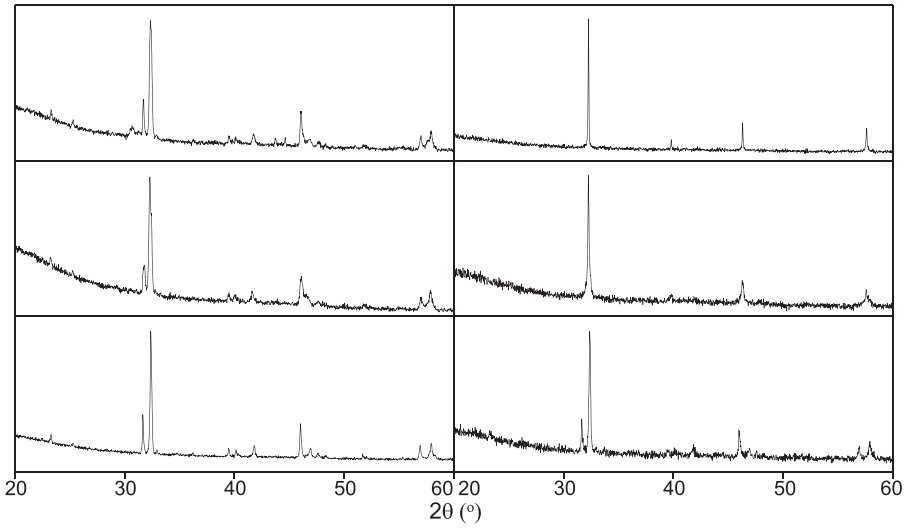

Fig. 4. X-ray diffraction patterns, from the bottom to the top, for $Sr_{0.75}Ca_{0.25}Fe_{0.95}Ge_{0.05}O_{3-\delta}$, $Sr_{0.75}Ca_{0.25}Fe_{0.90}Ge_{0.10}O_{3-\delta}$ and $Sr_{0.75}Ca_{0.25}Fe_{0.85}Ge_{0.15}O_{3-\delta}$, annealed at 800 (left) and 600 °C (right) for 24 h in 5%H_2–95%N_2.

(Ca,Sr)(Mn/Fe)O_3-based compounds were successfully doped with silicon [24–26]. In the case of such systems, the increase in cell parameters was correlated with the incorporation of Si leading to a reduction in the average Fe/Mn oxidation state due to the introduction of additional oxide ion vacancies as a result of the preference of Si to adopt tetrahedral coordination (see defect equation, in Kroger–Vink notation); the size increase due to this reduction in the average Fe/Mn oxidation state outweighing the effect of the smaller size of Si^{4+}.

$$SiO_2 + 3Fe_{Fe}^{X} + O_O^{X} \rightarrow Si_{Fe}^{X} + 2Fe_{Fe}^{'} + V_O^{\cdot\cdot} + 1/2O_2 + \text{“}FeO_2\text{”} \quad (1)$$

In the present case of Ge doping, the situation is slightly more complicated. In this case the ionic radii of Ge^{4+} and Fe^{4+} are similar, and Ge could potentially adopt either tetrahedral or octahedral coordination, the latter observed in $LaMg_{0.5}Ge_{0.5}O_3$. Nevertheless, the observation of a reduction in the average Fe oxidation states, from both TGA studies (Table 2) and the results obtained from the Mossbauer spectroscopy experiments, is consistent with an increase in oxygen vacancy content as the Ge content increases, and hence would suggest similar tetrahedral coordination for Ge. Further work (e.g. EXAFS studies) is required, however, to confirm this.

While the main focus of this study is on the potential applications as cathode materials for SOFCs, our prior work on Si doped $SrFeO_{3-\delta}$ suggested that there may also be potential applications as anode materials leading to the use in symmetrical fuel cells. With this in mind, the stability of the Ge doped materials was also examined under reducing conditions (24 h at 800 °C in 5% H_2–95%N_2). As previously reported [29], the undoped sample, $SrFeO_{3-\delta}$, showed a transition from a tetragonal to an orthorhombic symmetry under reducing conditions (see Fig. 3). This behaviour is due to the loss of oxygen, leading to the formation of a phase ($Sr_2Fe_2O_5$) with the brownmillerite structure and ordered oxygen vacancies. On Ge-doping we observe a stabilization of the cubic symmetry in reducing conditions for the highest germanium content ($x = 0.15$), although for lower germanium contents, the brownmillerite structure is formed. On increasing the Ca content the stabilisation of the cubic form is reduced, and for the $Sr_{0.75}Ca_{0.25}Fe_{1-x}Ge_xO_{3-\delta}$ series it was only possible to stabilize the cubic form for a germanium content equal to $x = 0.15$ at a lower temperature of 600 °C. For lower germanium contents at this temperature, and for all the Ge doped samples at 800 °C, the samples transformed to a brownmillerite structure in such reducing conditions (see Fig. 4).

3.2. ^{57}Fe Mössbauer spectroscopy

The ^{57}Fe Mössbauer spectra recorded from materials of composition $SrFe_{1-x}Ge_xO_{3-\delta}$ at 298 K are shown in Fig. 5. The ^{57}Fe Mössbauer parameters are collected in Table 3. The spectra at 298 K were best fitted to three quadrupole split absorptions. One component with chemical isomer shift ca. −0.05 mms^{-1} is characteristic of Fe^{5+} in perovskite-related structures [44–48]. The component with chemical isomer shift of ca. 0.37 mms^{-1} is characteristic of Fe^{3+} in octahedral coordination [49] and the doublet with chemical isomer shift ca. 0.18 mms^{-1} is typical of Fe^{3+} in lower than octahedral coordination [47]. The results are similar to those recorded at 298 K from $SrFe_{0.90}Si_{0.10}O_{3-\delta}$ where substitution of Fe^{4+} in $SrFeO_3$ by Si^{4+} caused disproportionation of the remaining Fe^{4+} into Fe^{5+} and Fe^{3+} [25]. Similar disproportionation has also been observed when Sn^{4+} is substituted [47,48] into $SrFeO_3$ and attributed to the dopant tetravalent ion causing lattice strain which can be mitigated by incorporating the smaller Fe^{5+} ions. The ^{57}Fe Mössbauer chemical isomer shift data (Table 3) which showed

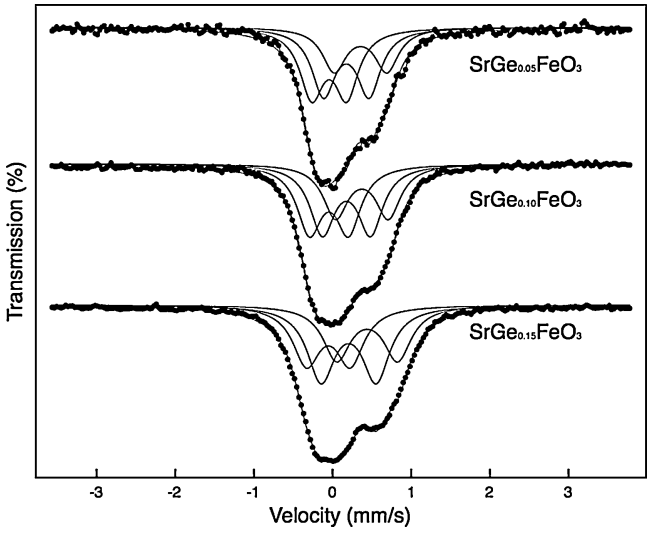

Fig. 5. ^{57}Fe Mössbauer spectra recorded for $SrFe_{1-x}Ge_xO_{3-\delta}$ series ($x = 0.05$, 0.10 and 0.15) at 298 K.

Table 3
^{57}Fe Mössbauer parameters for materials of composition $SrFe_{1-x}Ge_xO_{3-\delta}$.

x	T (K)	Assignment	IS ± 0.02 (mm s^{-1})	QS ± 0.02 (mm s^{-1})	H/T ± 0.05	Spectral area (%)
0.05	298	Fe^{5+}	−0.07	0.44	–	38
		Fe^{3+}	0.17	0.58	–	37
		Fe^{3+}	0.36	0.67	–	25
	20	Fe^{5+}	0.04	−0.08	26.5	52
		Fe^{3+}	0.48	−0.02	46.3	25
		Fe^{3+}	0.44	−0.01	43.1	23
0.10	298	Fe^{5+}	−0.05	0.50	–	35
		Fe^{3+}	0.18	0.61	–	37
		Fe^{3+}	0.37	0.67	–	28
	20	Fe^{5+}	0.01	−0.03	26.6	50
		Fe^{3+}	0.46	0.02	47.1	24
		Fe^{3+}	0.46	−0.04	44.0	26
0.15	298	Fe^{5+}	−0.05	0.56	–	30
		Fe^{3+}	0.20	0.70	–	40
		Fe^{3+}	0.44	0.77	–	30
	20	Fe^{5+}	−0.01	−0.13	26.5	39
		Fe^{3+}	0.47	0.01	48.9	20
		Fe^{3+}	0.47	−0.04	45.5	41

some Fe^{3+} ions to be in lower than octahedral coordination [49] implies oxygen deficiency around some Fe^{3+} ions in the $SrFe_{1-x}Ge_xO_{3-\delta}$ phases. The data also show the Fe^{3+} concentration to increase with increasing germanium substitution suggesting enhanced oxygen deficiency as the germanium content increases, as might be expected if it is accommodated as a tetrahedral ion.

The ^{57}Fe Mössbauer spectra recorded at 20 K are shown in Fig. 6 and the parameters are collected in Table 3. The spectra were significantly different from those recorded at 298 K and were best fitted to three sextets demonstrating that the materials magnetically order at temperatures between 298 and 20 K. One of the sextet components in each spectrum recorded at 20 K was characterised by a chemical isomer shift ca. 0.00 mm s^{-1} which we associate with the presence of Fe^{5+}. The other two sextets in each spectrum were characterised by chemical isomer shifts ca. 0.46 mm s^{-1} typical of Fe^{3+} at low temperatures.

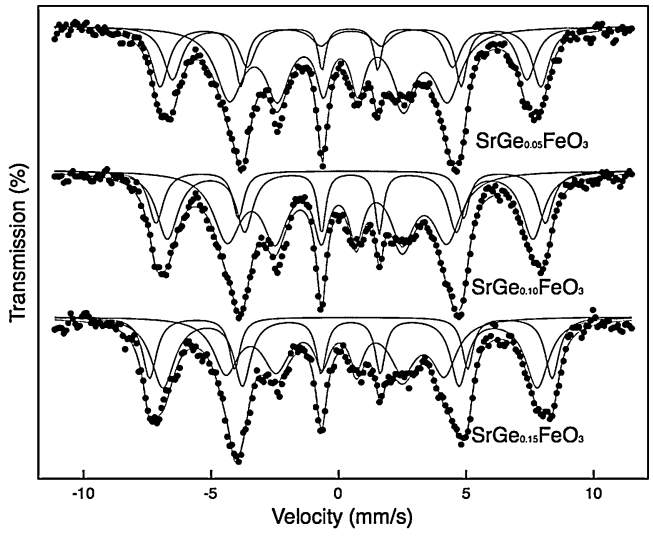

Fig. 6. ^{57}Fe Mössbauer spectra recorded from materials of composition $SrFe_{1-x}Ge_xO_{3-\delta}$ at 20 K.

3.3. Conductivity measurements

In this work, pellets for conductivity measurements were prepared at 1200 °C for 12 h, with densities for all the samples (doped and undoped) of ~85% theoretical.

a) In air

A significant decrease in the conductivity is observed for the $SrFe_{1-x}Ge_xO_{3-\delta}$ series on Ge doping (Fig. 7), while for the Ca doped series, $Sr_{1-y}Ca_yFe_{1-x}Ge_xO_{3-\delta}$, a small increase in the conductivity was observed. In these systems, the electrical property changes are most likely a balance between several factors: the disruptive effect of germanium on the electronic conduction pathway, the variation in the Fe oxidation state on Ge incorporation, and the effect of Ge doping on any oxygen vacancy ordering. Thus it is difficult to conclude the exact origin of these changes in conductivity, and further work would be needed in this respect to try to separate the effect of these various factors.

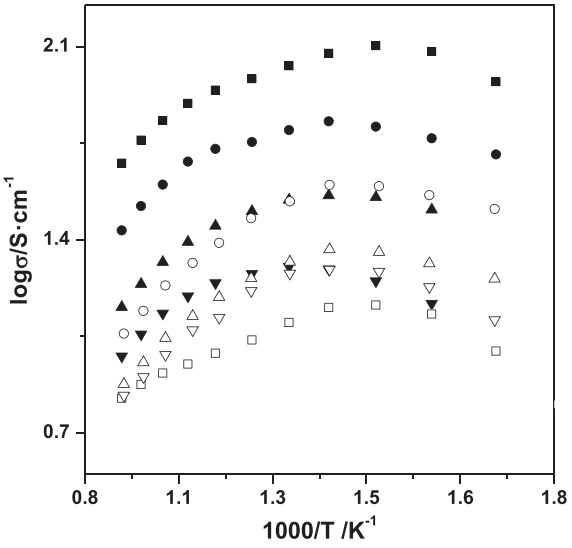

Fig. 7. Plot of logσ vs 1000/T for $SrFeO_{3-\delta}$ (■), $SrFe_{0.95}Ge_{0.05}O_{3-\delta}$ (●), $SrFe_{0.90}Ge_{0.10}O_{3-\delta}$ (▲), $SrFe_{0.85}Ge_{0.15}O_{3-\delta}$ (▼), $Sr_{0.75}Ca_{0.25}FeO_{3-\delta}$ (□), $Sr_{0.75}Ca_{0.25}Fe_{0.95}Ge_{0.05}O_{3-\delta}$ (○), $Sr_{0.75}Ca_{0.25}Fe_{0.90}Ge_{0.10}O_{3-\delta}$ (△) and $Sr_{0.75}Ca_{0.25}Fe_{0.85}Ge_{0.15}O_{3-\delta}$ (▽).

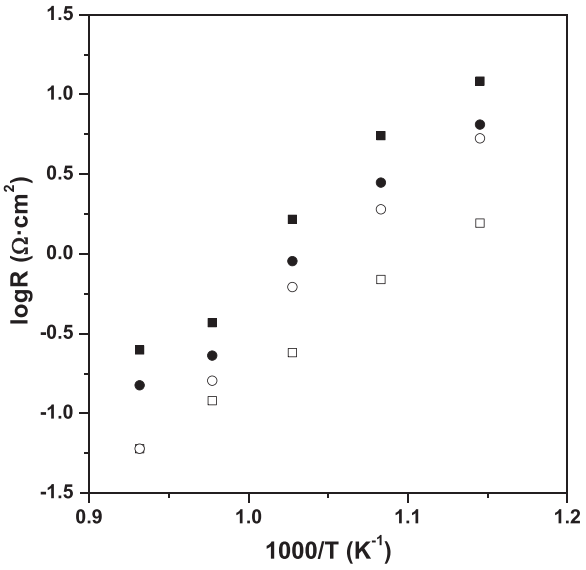

Fig. 8. Plot of log (area-specific resistance (ASR)) vs 1000/T for $SrFeO_{3-\delta}$ (■), $SrFe_{0.85}Ge_{0.15}O_{3-\delta}$ (□), $Sr_{0.75}Ca_{0.25}FeO_{3-\delta}$ (●) and $Sr_{0.75}Ca_{0.25}Fe_{0.85}Ge_{0.15}O_{3-\delta}$ (○).

All samples showed a change in the conductivity plot above ~400 °C, which can be attributed to oxygen loss at these higher temperatures reducing the average Fe oxidation state, and hence the electronic charge carriers.

b) In $5\%H_2/N_2$

Following the positive results obtained in the stability experiments in $5\%H_2/N_2$ the conductivities of the $SrFe_{1-x}Ge_xO_{3-\delta}$ series were measured in this atmosphere. The results for $SrFe_{0.95}Ge_{0.05}O_{3-\delta}$ and $SrFe_{0.9}Ge_{0.1}O_{3-\delta}$ showed very low conductivity values, as well as a transition from a cubic perovskite to a brownmillerite structure. For $SrFe_{0.85}Ge_{0.15}O_{3-\delta}$ the sample remained cubic after the experiment, however, the conductivity values were still very low, 0.09 and 0.04 S cm^{-1} at 800 and 700 °C, respectively. Given these low conductivity values, such systems could not be used on their own as SOFC anodes. However, they could potentially be used in cermets with the introduction of Ni or Cu to increase the electronic conductivity.

3.4. Area-specific resistance study

Following the conductivity results, cathode testing was performed for these samples. These experiments used a composite of the perovskite and CGO10 (1:1 wt%) on dense CGO10 pellets. The composite was deposited at 900 °C, and at this temperature there was no evidence of any segregation of secondary phases in perovskite-CGO10 mixtures.

The dependencies of the ASR values in air with temperature are shown in Fig. 8 and Table 2. For instance, for $SrFe_{0.85}Ge_{0.15}O_{3-\delta}$ and $Sr_{0.75}Ca_{0.25}Fe_{0.85}Ge_{0.15}O_{3-\delta}$, the values obtained at 700 °C, were 0.24 and 0.62 Ω cm^2, respectively. In comparison, the results for the undoped samples, $SrFeO_{3-\delta}$ and $Sr_{0.75}Ca_{0.25}FeO_{3-\delta}$, were 1.65 and 0.91, respectively, indicating a significant improvement on Ge doping. Therefore, despite the decrease in the electronic conductivity values on Ge-doping for the $SrFe_{1-x}Ge_xO_{3-\delta}$ series, we see an improvement in the ASR values, possibly related to the generation of oxygen vacancies and an increase in the oxide conductivity of the cathode material. The ASR data show a non-linear behaviour with temperature, with a bigger decrease in the values at the higher temperatures. This behaviour is likely due to the fact that these systems show loss of oxygen at high temperature, causing an increase in oxide vacancies and hence a better oxide ion mobility and lower ASR values at the higher temperatures. Further work is required to investigate the effect of synthesis temperature (e.g. the use of lower temperature sol gel routes) of the electrode materials on the performance, since particle size and microstructure will also have a significant effect on performance.

4. Conclusions

In $Sr_{1-y}Ca_yFe_{1-x}Ge_xO_{3-\delta}$ perovskite materials with Ca contents $y < 0.5$, prepared by solid state reaction, X-ray diffraction data have shown that doping with germanium results in a change from tetragonal to cubic symmetry, which we have attributed to an increase in disorder on the oxygen sublattice, although neutron diffraction studies are required to add further confirmation. With higher calcium contents, $y \geq 0.5$, it was not possible to achieve full stabilization of the cubic symmetry through Ge doping. Annealing experiments in $5\%H_2/95\%N_2$ also showed the stabilization of the cubic form for the Ge-doped $SrFeO_{3-\delta}$ at high (15 mol%) Ge doping levels under these reducing conditions. Composite cathodes with 50 wt% $Ce_{0.9}Gd_{0.1}O_{1.95}$ were examined on dense $Ce_{0.9}Gd_{0.1}O_{1.95}$ pellets in air. An improvement in the area specific resistances (ASR) values was observed for the Ge-doped samples, suggesting a beneficial effect from the Ge doping on the electrode performance. Thus, these results indicate that germanium can be incorporated into perovskite ferrites and can have a beneficial effect on the performance, suggesting that its use as a dopant may potentially be extended to other areas where perovskite systems are attracting interest.

Acknowledgements

We would like to express thanks to EPSRC for funding (grants EP/I003932) and to the Spanish Ministry of Economy and Competitiveness for its financial support under project MAT2012-38045-C04-01. The Bruker D8 diffractometer and Netzsch STA 449 F1 Jupiter Thermal Analyser used in this research were obtained through the Science City Advanced Materials project: Creating and Characterising Next generation Advanced Materials project, with support from Advantage West Midlands (AWM) and part funded by the European Regional Development Fund (ERDF).

References

[1] A. Orera, P.R. Slater, Chem. Mater. 22 (2010) 675.
[2] A.J. Jacobson, Chem. Mater. 22 (2010) 660.
[3] A. Lashtabeg, S.J. Skinner, J. Mater. Chem. 16 (2006) 3161.
[4] A. Martínez-Amesti, A. Larranaga, L.M. Rodríguez-Martínez, A.T. Aguayo, J.L. Pizarra, M.L. Nóa, A. Laresgoiti, M.I. Arriortua, J. Power Sources 185 (2008) 401.
[5] D. Kuscer, D. Hanzel, J. Holc, M. Hrovat, D. Kolar, J. Am. Ceram. Soc. 84 (2001) 1148.
[6] C. Greaves, P.R. Slater, J. Mater. Chem. 1 (1) (1991) 17.
[7] C. Greaves, P.R. Slater, Physica C 175 (1991) 172.
[8] P.R. Slater, C. Greaves, M. Slaski, C.M. Muirhead, Physica C 208 (1993) 193.
[9] Y. Miyazaki, H. Yamane, N. Ohnishi, T. Kajitani, K. Hiraga, Y. Mori, S. Funahashi, T. Hirai, Physica C 198 (1992) 7.
[10] A. Maignan, M. Hervieu, C. Michel, B. Raveau, Physica C 208 (1993) 116.
[11] K. Kinochita, T. Yamada, Nature 357 (1992) 313.
[12] B. Raveau, M. Hervieu, D. Pelloquin, C. Michel, R. Retoux, Z. Anorg, Allg. Chem. 631 (2005) 1831.
[13] D. Pelloquin, M. Hervieu, C. Michel, N. Nguyen, B. Raveau, J. Solid State Chem. 134 (1997) 395.
[14] V. Caignaert, B. Domenges, B. Raveau, J. Solid State Chem. 120 (1995) 279.
[15] J.F. Shin, L. Hussey, A. Orera, P.R. Slater, Chem. Commun. 46 (2010) 4613.
[16] J.F. Shin, D.C. Apperley, P.R. Slater, Chem. Mater. 22 (2010) 5945.
[17] J.F. Shin, P.R. Slater, J. Power Sources 196 (2011) 8539.
[18] J.F. Shin, K. Joubel, D.C. Apperley, P.R. Slater, Dalton Trans. 41 (2012) 261.
[19] C.A. Hancock, R.C.T. Slade, J.R. Varcoe, P.R. Slater, J. Solid State Chem. 184 (2011) 2972.
[20] J.M. Porras-Vazquez, P.R. Slater, J. Power Sources 209 (2012) 180.
[21] J.M. Porras-Vazquez, T.F. Kemp, J.V. Hanna, P.R. Slater, J. Mater. Chem. 22 (2012) 8287.
[22] J.M. Porras-Vazquez, P.R. Slater, Fuel Cells 12 (2012) 1056.

[23] C.A. Hancock, P.R. Slater, Dalton Trans. 40 (2011) 5599.
[24] J.M. Porras-Vazquez, E.R. Losilla, P.J. Keenan, C.A. Hancock, T.F. Kemp, J.V. Hanna, P.R. Slater, Dalton Trans. 42 (2013) 5421.
[25] J.M. Porras-Vazquez, T. Pike, C.A. Hancock, J.F. Marco, F.J. Berry, P.R. Slater, J. Mater. Chem. A 1 (2013) 11834.
[26] J.M. Porras-Vazquez, R.I. Smith, P.R. Slater, J. Solid State Chem. 213 (2014) 132.
[27] U.W. Blass, F. Langenhorst, T. Boffa-Ballaran, F. Seifert, D.J. Frost, C.A. McCammon, Phys. Chem. Miner. 31 (2004) 52.
[28] M. Murakami, K. Hirose, K. Kawamura, N. Sata, Y. Ohishi, Science 304 (2004) 855.
[29] A.R. Oganov, S. Ono, Nature 430 (2004) 445.
[30] A.R. Oganov, R. Martonak, A. Laio, P. Raiteri, M. Parrinello, Nature 438 (2005) 1142.
[31] W.S. Xiao, D.Y. Tan, W. Zhou, M. Chen, X.L. Xiong, M. Song, J. Liu, H.K. Ma, J. Xu, Am. Mineral. 97 (2012) 1193.
[32] P. Nemeth, K. Leinenweber, T.L. Groy, P.R. Buseck, Am. Mineral. 92 (2007) 441.
[33] M. Swaffer, P.R. Slater, R.K.B. Gover, T. Matsumura, R. Kanno, T. Kamiyama, Chem. Commun. (2002) 1176.
[34] J. Yoo, A. Verma, S. Wang, S. Jacobson, J. Electrochem. Soc. 152 (2005) A497.
[35] V. Zaspalis, A. Evdou, L. Nalbandian, Fuel 89 (2010) 1265.
[36] Y. Niu, W. Zhou, J. Sunarso, L. Ge, Z. Zhu, Z. Shao, J. Mater. Chem. 20 (2010) 9619.
[37] J.P. Hodges, S. Short, J.D. Jorgensen, X. Xiong, B. Dabrowski, S.M. Mini, C.W. Kimball, J. Solid State Chem. 151 (2000) 190.
[38] V. Vashuk, L. Kokhanovskii, I. Yushkevich, Inorg. Mater. 36 (2000) 79.
[39] M.V. Patrakeev, I.A. Leonidov, V.L. Kozhevnikov, V.V. Kharton, Solid State Sci. 6 (2004) 907.
[40] P. Adler, A. Lebon, V. Damljanovic, C. Ulrich, C. Bernhard, A.V. Boris, A. Maljuk, C.T. Lin, B. Keimer, Phys. Rev. B 73 (2006) 094451.
[41] M. Schmidt, S.J. Campbell, J. Solid State Chem. 156 (2001) 292.
[42] A.C. Larson, R.B.V. Dreele, General Structure Analysis System (GSAS) program. Rep. No. LA-UR-86748, Los Alamos National Laboratory, Los Alamos, CA, 1994.
[43] D. Johnson, ZView: A Software Program for IES Analysis, Version 2.8, Scribner Associates, Inc., Southern Pines, NC, 2008.
[44] P. Adler, J. Solid State Chem. 130 (1997) 129.
[45] S.E. Dann, M.T. Weller, D.B. Currie, M.F. Thomas, A.D. Al-Rawas, J. Mater. Chem. 3 (1993) 1231.
[46] G.S. Case, A.L. Hector, W. Levason, R.L. Needs, M.F. Thomas, M.T. Weller, J. Mater. Chem. 9 (1999) 2821.
[47] G. Demazaeau, P. Fabritchnyi, L. Fournes, S. Darracq, I.A. Presniakov, K.V. Pokholok, V.P. Gorkov, J. Etourneau, J. Mater. Chem. 5 (1995) 553.
[48] F.J. Berry, A.F. Bowfield, F.C. Coomer, S.D. Jackson, E.A. Moore, P.R. Slater, M.F. Thomas, A.J. Wright, X. Ren, J. Phys.: Condens. Matter 21 (2009) 256001.
[49] F. Menil, J. Phys. Chem. Solids 46 (1985) 763.